Supporting Information

Smith et al. 10.1073/pnas.1101920108

SI Materials and Methods

Profile Analysis. Profile analysis was conducted on all recorded neurons using the method by Tindell et al. (1) (Fig. S2). We denoted each neuron's firing rate (normalized to baseline) to conditioned stimulus (CS)+1, CS+2, and unconditioned stimulus (UCS) as x, y, and z, respectively. The relative rank ordering of these three numbers according to their magnitude represents the profile of a neuron's responses to the stimuli. For each neuron, we constructed a 2D vector (α and β), where $\alpha = (2y - x - z)/2\beta = \sqrt{3}(x - z)/2$. The α and β components capture the two orthogonal contrasts formed among the three dependent variables x, y, and z such that any other contrast is a rotation in the 2D space. This vector's magnitude $r = \sqrt{(\alpha^2 + \beta^2)} = \sqrt{[(x-y)^2 + (y-z)^2 + (z-x)^2]/2}$ represents the extent to which the neuron's firing rates, x, y, and z are differentially modulated by the three types of stimuli (CS+1, CS+2, and UCS). The vector's direction $\theta = \tan^{-1}(\beta/\alpha)$ reflects the rank ordering of the magnitudes of these firing rates in the unit's response profile. Each unit's profile vector was calculated based on responses to the three stimuli (CS+1, CS+2, and UCS). For comparing populations, we computed distributions of neurons in profile space and population profile vectors. Distributions were determined by counting the number of unit profile vectors in each of 12 bins 30° wide (the 0° bin consists of all those units with directional angles between −15° and 15°, the 90° bin consists of all those units with angles between 75° and 105°, etc.). Population profile vectors were computed as the vector sum of individual unit profile vectors (i.e., α, β values). The population profile vector represents the overall population responses to the three stimuli (CS+1, CS+2, and UCS). The angular directions of the population profile vector reflect the relative rank order of the magnitude of the firing responses to these stimuli, whereas vector lengths represent the variance of the responses across the three stimuli. Thus, this analysis provides a computational approach to comparing three possible coding schemes within ventral pallidum (VP) neurons: maximal predictive signal (in which the population profile vector occupies CS+1 space at 60°–180°), maximal incentive signal (CS+2 space at −60° to 60°), and maximal hedonic signal (UCS space at −180° to −60°) (Fig. S2).

Bursting Analysis. A software program written in the laboratory (EpochBuilder) extracted the spikes for the epochs in each trial, and it computed average interspike interval and identified bursts using the surprise method of Legendy and Salcman (2). This procedure calculates a surprise value defined as the "negative logarithm of the probability of the occurrence of a burst in a random (Poisson) spike train" (2). Bursts have a minimum of two successive intervals (three spikes). When at least two intervals with a mean duration of one-half the mean background interval length of the unit were found, a surprise value was calculated. Additional spikes (up to 10) were then added iteratively to the end of the burst, recomputing the surprise value with each spike addition to maximize its value. After the addition procedure reached a maximum, a subtraction, one spike at a time, from the beginning of the burst (maintaining at least three) was repeated iteratively to again maximize the surprise value. After the burst's surprise value has been maximized, the value was compared with the minimum acceptable surprise value to define a burst. This value is set to a surprise value of three (i.e., a probability of 1 in 1,000). The search for the next burst then resumes at the spike immediately after the burst or at the second spike of the candidate burst, if the candidate is rejected for failing to meet the threshold requirement. The algorithm allows a burst to occur immediately after a burst, but bursts may not overlap. Background (intertrial) interval lengths were defined as the average interval length in prestimulus periods. The duration and surprise value for each burst was recorded as well as the unit and epoch to which it belonged. Because both the number of bursts and the surprise value are indicative of the bursting properties of each cell, the burst index method of Aldridge and Gilman (3) was used to enable comparisons of bursting between units. The burst index was calculated by taking the square root of the product of the number of bursts per 1,000 spikes and the average surprise value within that epoch and unit. All analysis data were stored in a computerized database and analyzed using ANOVAs.

Fos Plume Analysis and Functional Microinjection Mapping. We assessed the extent of functional spread of drug microinjection in the nucleus accumbens (NAc) using a Fos plume mapping technique using procedures from previous studies designed to maximize accuracy in measurement (4–9). The spread of drug-induced neuronal activation can be estimated by increases in plumes of Fos expression around the site of microinjection and comparisons with vehicle injections or uninjected tissue. It is important not to underestimate plume size to avoid overly precise localization of function, which could occur if plumes shrank from gliosis after several microinjections. Thus, plumes were assessed in separate animals (n = 10). After calculating a 3D mean volume of maximal Fos activation caused by each drug in these animals, we used those measured volumes to construct functional maps of individual NAc microinjections and their affect on VP event-related firing from animals in the main experiment (Fig. S1).

Specifically, [D-Ala2, N-MePhe4, Gly-ol]-enkephalin (DAMGO), amphetamine, or artificial cerebral spinal fluid (ACSF) were microinjected into the medial NAc shell at the same dose, volume, and rate at sites that coincided with placements in the group of animals tested for behavior and VP firing. Ninety minutes after drug microinjection, rats were deeply anesthetized with sodium pentobarbital before transcardial perfusion (10). Brains were removed and placed in 4% formaldehyde for 2 h, placed in 30% sucrose overnight, and then, sectioned at 60 μm and stored in 0.2 M NaPb (pH 7.4). The avidin-biotin procedure was used to visualize Fos-like immunoreactivity (11). Brain sections were immersed in blocking solution [3% normal goal serum and 0.3% Triton X-100 in Tris phosphate buffered saline (TPBS)] for 1 h and then incubated at room temperature for 24 h with a rabbit polyclonal antiserum directed against the N-terminal region of the Fos gene (dilution of 1:5,000 in triton PBS, 1% normal goat serum, and 0.3% Triton X-100; Sigma). The antiserum was preabsorbed with acetone-dried rat liver powder overnight at 4 °C. After the primary antibody incubation, sections were exposed to goat anti-rabbit and biotinylated secondary IgG (diluted 1:200; Santa Cruz) and then, to avidin-biotin-peroxidase complex for 1 h at room temperature. A nickel diaminobenzidine (nickel-DAB) glucose oxidase reaction was used to visualize Fos-like immunoreactive cells. Sections were washed in Tris buffer, mounted from PBS, air-dried, dehydrated in alcohol, cleared in xylene, and coverslipped. Fos-like immunoreactivity was assessed using a Leica microscope coupled to a SPOT RT slider (Diagnostic Instruments) using SPOT software (SPOT version 3.3).

Measured radii of Fos plumes were used to calculate the volumes of local drug activation spheres and map functional consequences onto the cannula sites (at equivalent locations) used for behavioral tests (Fig. S1). Using previous methods for Fos plume analyses (4, 5, 7–9), Fos-labeled cells were counted individually within blocks (125 × 125 μm) on tissue surface with 5–40× magnification at point locations spaced at 125-μm intervals along each of the seven radial arms emanating from the center of the microinjection site (45°, 90°, 135°, 180°, 225°, 270°, and 315°). For microinjection sites, Fos densities were measured (*i*) in normal tissue of brains without a microinjection cannula to assess normal baseline expression, (*ii*) around the site of vehicle microinjections to assess cannula track and vehicle-induced Fos baseline expression, and (*iii*) around the local site of drug microinjections to assess drug-induced changes in Fos caused by DAMGO or amphetamine. Fos plumes surrounding drug microinjections were partitioned into zones of intense vs. moderate Fos levels. Intense and moderate zones were identified in two ways: (*i*) as absolute increases over normal levels [elevation by 10 (intense) or 5 times (moderate) normal tissue counts sampled in the absence of any cannula track] and (*ii*) as vehicle-relative increases caused by drug (elevation five or two times over vehicle microinjection-induced levels at equivalent point locations around drug vs. vehicle microinjection tracks).

The calculated mean area of intense increase in Fos expression per drug derived from these data was then used to aid anatomical mapping of functional effects on VP firing caused by NAc microinjections in the main experiment. Each microinjection was plotted using its histologically identified location in the NAc with a symbol sized according to the mean area of intense Fos activation caused by that drug in the separate animals and a color-coding scheme to reflect the effect of that particular microinjection on changes of task-related neuronal firing recorded in the VP on that test day (Fig. S1).

SI Results

Fos Plumes. Fos plumes after DAMGO microinjection were measured as: 10× normal = 0.16 mm radius, 0.0037 mm^3; 5× normal = 0.73 mm radius, 0.38 mm^3; 2× normal = 1.12 mm radius, 1.40 mm^3; 5× vehicle = 0.46 mm radius, 0.10 mm^3; 2× vehicle = 0.99 mm radius, 0.96 mm^3. Amphetamine microinjection caused a similar intense Fos plume of 10× normal activation at the tip of the injection (10× normal = 0.23 ± 0.04 mm radius, 0.012 mm^3 volume) and a moderate to low intensity of Fos elevation in a larger surrounding area (5× normal = 0.68 ± 0.08 mm radius, 0.32 mm^3; 2× normal = 0.94 ± 0.12 mm radius, 0.84 mm^3; 5× vehicle = 0.34 ± 0.04 mm radius, 0.039 mm^3; 2× vehicle = 0.89 ± 0.12 mm radius, 0.72 mm^3) (Fig. S1).

Conditioned Behavioral Alerting Reactions to Serial Cues. Behavioral alerting reactions (head turn, step, and rear) were also assessed in the first 2 s of the CS+ and CS− tones, and they were analyzed in a binary measure of reacted or failed to react. Reaction occurrence was increased to the CS+1 tone with all drugs and vehicle compared with CS− (vehicle: $F_{1,153} = 33.64$, $P < 0.05$; DAMGO: $F_{1,134} = 7.50$, $P < 0.05$; amphetamine: $F_{1,154} = 41.26$, $P < 0.05$) as well as increased to the CS+2 tone compared with CS− (vehicle: $F_{1,153} = 17.61$, $P < 0.05$; DAMGO: $F_{1,134} = 4.75$, $P < 0.05$; amphetamine: $F_{1,155} = 16.20$, $P < 0.05$). Animals reacted to the CS+2 slightly less compared with CS+1 after vehicle and DAMGO microinjection and significantly less after amphetamine (vehicle: $F_{1,159} = 2.03$, NS; DAMGO: $F_{1,133} = 0.29$, NS; amphetamine: $F_{1,156} = 4.27$, $P < 0.05$), perhaps as a result of masking from alerting reactions already evoked by CS+1 or its predictive redundancy. Furthermore, DAMGO microinjection increased CS+2 alerting reactions over vehicle to the CS+2 ($F_{1,146} = 3.30$, $P = 0.07$) but not to the CS+1 (DAMGO: $F_{1,146} = 1.02$, NS), and also, it increased reactions to the CS− over vehicle levels ($F_{1,141} = 12.99$, $P < 0.05$). Amphetamine microinjection did not affect reaction amount compared with vehicle for any particular CS (CS+1: $F_{1,157} = 1.84$, NS; CS+2: $F_{1,158} = 0.50$, NS ; CS−: $F_{1,150} = 0.83$, NS).

1. Tindell AJ, Berridge KC, Zhang J, Peciña S, Aldridge JW (2005) Ventral pallidal neurons code incentive motivation: Amplification by mesolimbic sensitization and amphetamine. *Eur J Neurosci* 22:2617–2634.
2. Legéndy CR, Salcman M (1985) Bursts and recurrences of bursts in the spike trains of spontaneously active striate cortex neurons. *J Neurophysiol* 53:926–939.
3. Aldridge JW, Gilman S (1991) The temporal structure of spike trains in the primate basal ganglia: Afferent regulation of bursting demonstrated with precentral cerebral cortical ablation. *Brain Res* 543:123–138.
4. Peciña S, Berridge KC (2000) Opioid site in nucleus accumbens shell mediates eating and hedonic 'liking' for food: Map based on microinjection Fos plumes. *Brain Res* 863: 71–86.
5. Peciña S, Berridge KC (2005) Hedonic hot spot in nucleus accumbens shell: Where do mu-opioids cause increased hedonic impact of sweetness? *J Neurosci* 25:11777–11786.
6. Smith KS, Berridge KC (2007) Opioid limbic circuit for reward: Interaction between hedonic hotspots of nucleus accumbens and ventral pallidum. *J Neurosci* 27: 1594–1605.
7. Mahler SV, Smith KS, Berridge KC (2007) Endocannabinoid hedonic hotspot for sensory pleasure: Anandamide in nucleus accumbens shell enhances 'liking' of a sweet reward. *Neuropsychopharmacology* 32:2267–2278.
8. Faure A, Reynolds SM, Richard JM, Berridge KC (2008) Mesolimbic dopamine in desire and dread: Enabling motivation to be generated by localized glutamate disruptions in nucleus accumbens. *J Neurosci* 28:7184–7192.
9. Smith KS, Berridge KC (2005) The ventral pallidum and hedonic reward: Neurochemical maps of sucrose "liking" and food intake. *J Neurosci* 25:8637–8649.
10. Herrera DG, Robertson HA (1996) Activation of c-fos in the brain. *Prog Neurobiol* 50: 83–107.
11. Hsu SM, Raine L, Fanger H (1981) Use of avidin-biotin-peroxidase complex (ABC) in immunoperoxidase techniques: A comparison between ABC and unlabeled antibody (PAP) procedures. *J Histochem Cytochem* 29:577–580.

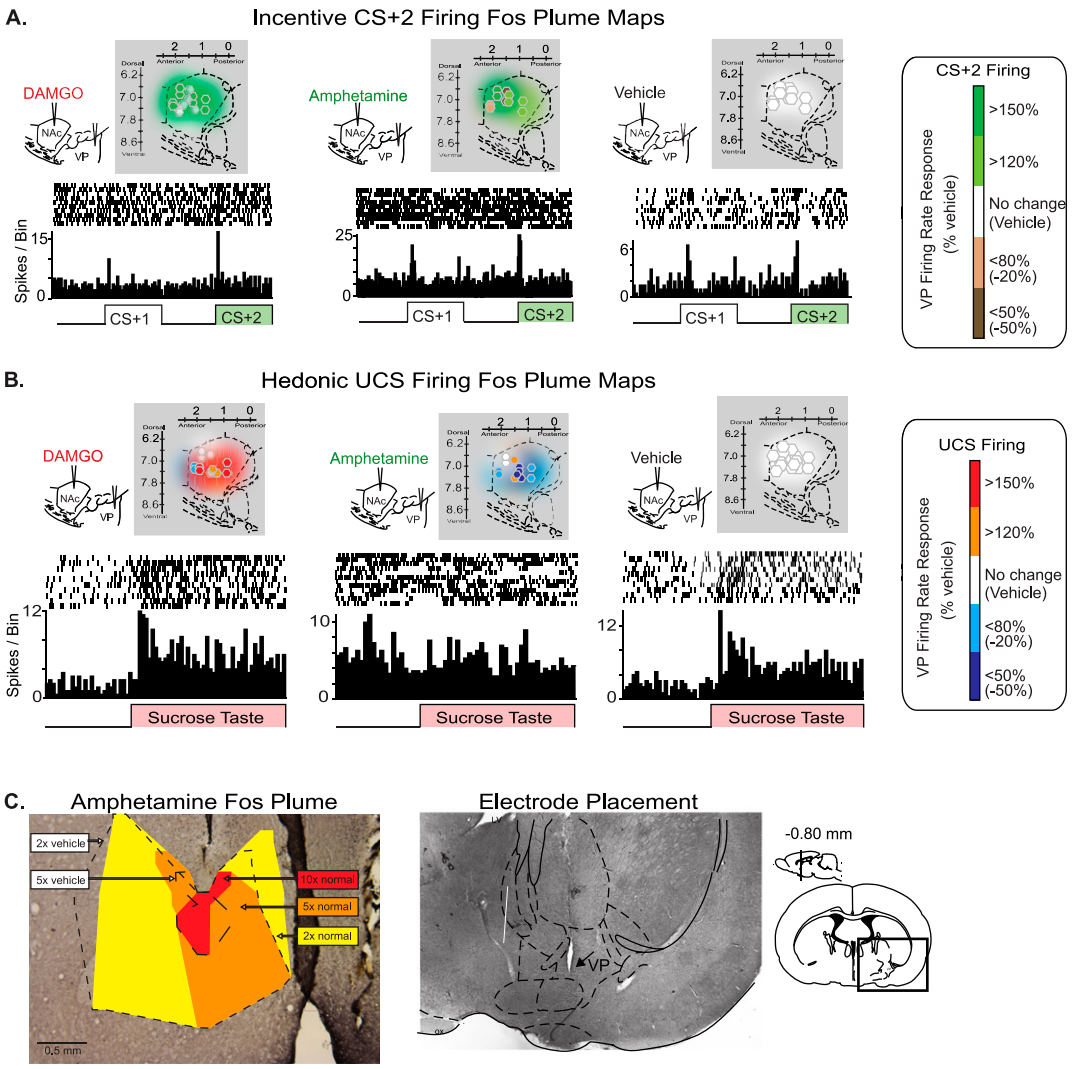

Fig. S1. Fos plume maps of NAc microinjection effects on VP "wanting" and "liking" signals. (*A*) Colored Fos plume maps show vehicle-subtracted enhancement of firing to the incentive CS+2 (symbols show each injection placement sized by Fos spread measures; colors show firing compared with vehicle: green, enhanced; brown, suppressed; white, no change). Vehicle subtracted from itself shown for comparison. Microinjection plume locations are shown over a sagittal outline of the NAc. Representative perievent raster and histogram for single VP neurons are shown below. (*B*) Hedonic Fos plume map shows enhancement of firing to the UCS after DAMGO (red) and trend to hedonic suppression after amphetamine (blue). Perievent raster histograms show example neuronal responses to the UCS. (*C Left*) Fos plumes provide an estimation of the anatomical spread where a drug microinjection acted in the NAc to cause functional effects. In this example (coronal image at 5× magnification), amphetamine microinjection in the dorsal medial shell of the NAc caused a small inner plume of intense Fos activation (red, zone of 10× normal uninjected tissue surrounded by wider halo zones of intermediate or low Fos activation; orange, 5× normal; yellow, 2× normal; broad dashed line, 5× vehicle; thin dashed line, 2× vehicle). (*C Right*) Example electrode placement in the hedonic hotspot in the posterior VP (here showing placement at −0.8 mm to bregma; 5× magnification).

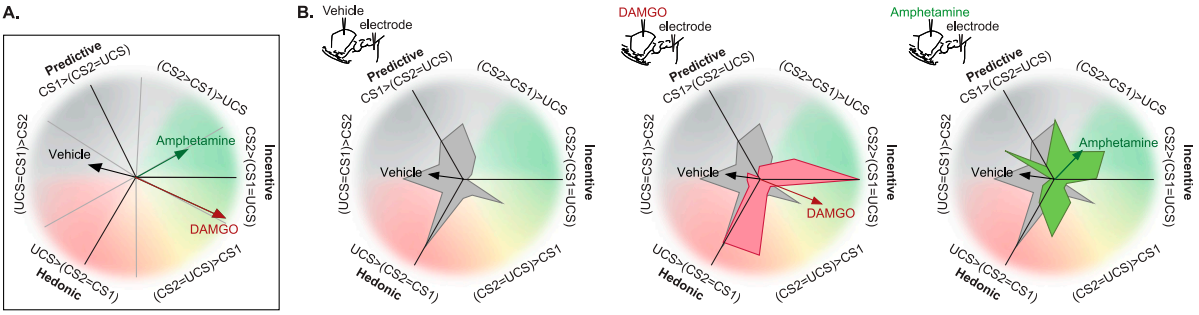

Fig. S2. Profile analysis of VP firing reveals that amphetamine and DAMGO in the NAc both enhanced incentive signals but only DAMGO additionally enhanced hedonic signals. Arrows in *A* and *B* show firing preference of the VP neuronal population expressed as highest firing to incentive CS+2 and predictive CS+1 vs. hedonic UCS. Underlying color grids in *B* also show the population distribution where each recorded neuron fell within response profile space (greater distance from center equals larger number of neurons with that profile). Normally under vehicle (gray), VP neurons fired maximally to the CS+1, reflecting prediction bias. DAMGO microinjection (red) caused the firing bias to shift to both UCS "liking" and CS+2 "wanting." Amphetamine shifted firing selectively to CS+2 (green) and did not enhance UCS firing. Prediction-related CS+1 firing was not enhanced by either drug, and therefore, declined in relative magnitude to other stimuli after NAc stimulation. Firing rates for *A* were compared for peak CS and UCS response windows (CS = 0–0.5 s; UCS = 1–1.5 s) in only the first five trials to best equate stimuli; firing rates in *B* were compared across all trials.

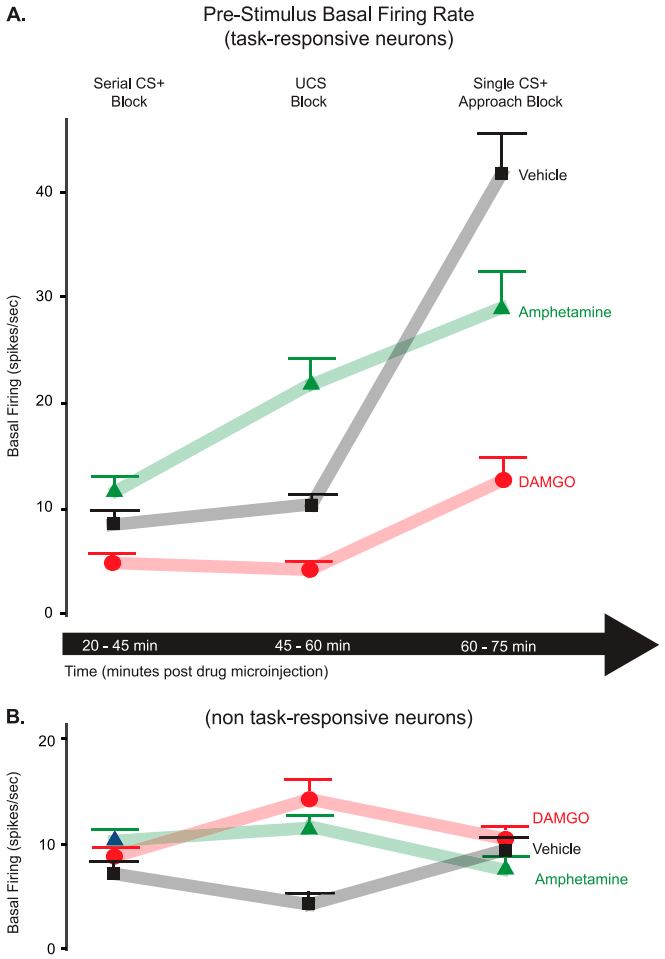

Fig. S3. Modulation of baseline firing rate by NAc microinjection and task context. (*A*) Task-responsive neurons. NAc microinjection of amphetamine enhanced, whereas DAMGO suppressed VP firing in the 5-s period preceding the CS+1 (first test: 20–45 min postinjection) and also the UCS (second test: 45–60 min postinjection) compared with vehicle. Later, in the single CS+ Pavlovian test (60–75 min postinjection), baseline firing rate in the 5 s preceding the feeder click climbed in all drug conditions but most dramatically in the vehicle condition. However, notably, drug-evoked increases in firing to stimuli were independent of these fluctuating baselines (e.g., both drugs enhanced CS+-evoked firing in the initial serial test and late single approach test). (*B*) Neurons not responsive to task events showed distinct levels of basal firing that were generally unchanged across drug conditions, with the exception of higher firing in the pre-UCS period after DAMGO or amphetamine.

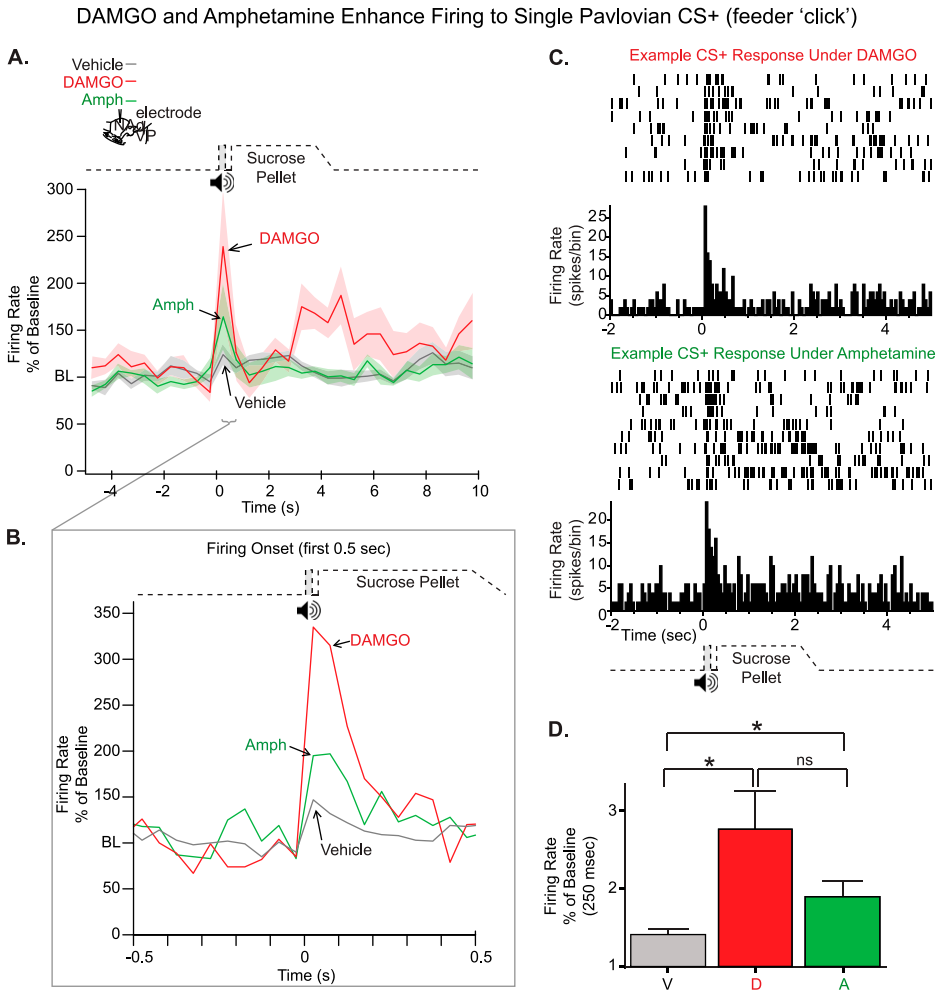

Fig. S4. Naturalistic Pavlovian approach experiment containing a single auditory CS+ that combined predictive and incentive components into one signal paired with UCS of sugar pellet delivery. (*A* and *B*) NAc DAMGO (red) and amphetamine (green) microinjection both enhanced the burst of VP neuronal firing to the single feeder click CS+ that preceded the delivery of a sucrose pellet and evoked a behavioral approach conditioned response to the sucrose dish. Lines represent mean firing in 0.5- (*A*) or 0.1-s (*B*) windows calculated as a percentage of prestimulus baseline as in Fig. 2. (*C*) Raster and histogram plots show example rapid and phasic excitation of VP firing to the CS+ (at time 0) after DAMGO or amphetamine microinjection in the NAc. (*D*) Bar graph representation of significant firing increases to the click within 250 ms. *$P < 0.05$ amphetamine or DAMGO firing compared with vehicle.

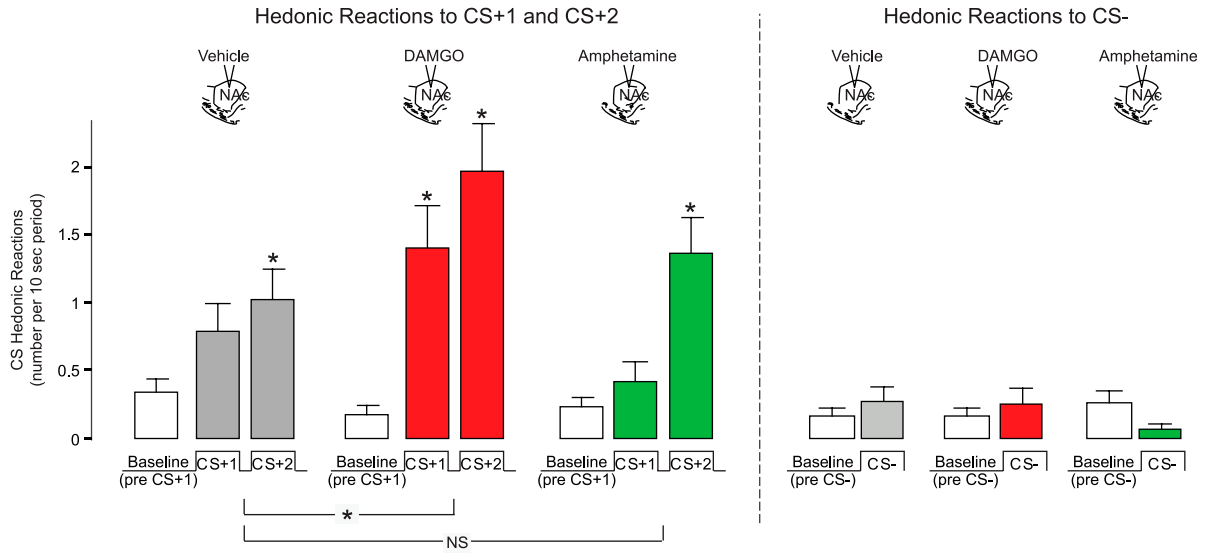

Fig. S5. Behavioral hedonic "liking" reactions to auditory stimuli. (*Left*) Conditioned hedonic reactions evoked by the CS+1 or CS+2 were raised above baseline (to approximately one reaction) and enhanced by DAMGO (to approximately two reactions) but not amphetamine. (*Right*) The very rare reactions to the CS– predicting nothing were unaffected by NAc microinjection. *$P < 0.05$.

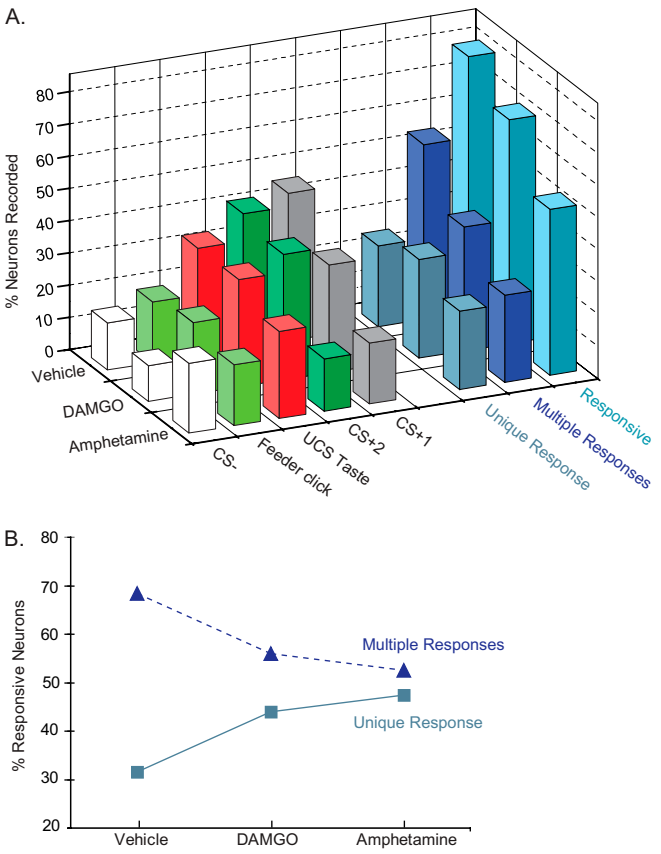

Fig. S6. NAc opioid or dopamine stimulation narrows the stimulus focus of active VP neuronal populations. (*A*) The proportion of responsive neurons decreased with amphetamine and DAMGO stimulation of the NAc, with some variations across stimuli. (*B*) Of responsive neurons, the relative proportion of neurons responding to only one stimulus increased (e.g., only CS+1, only CS+2, only UCS, or only single CS+), whereas the number of neurons responsive to two or more stimuli decreased.

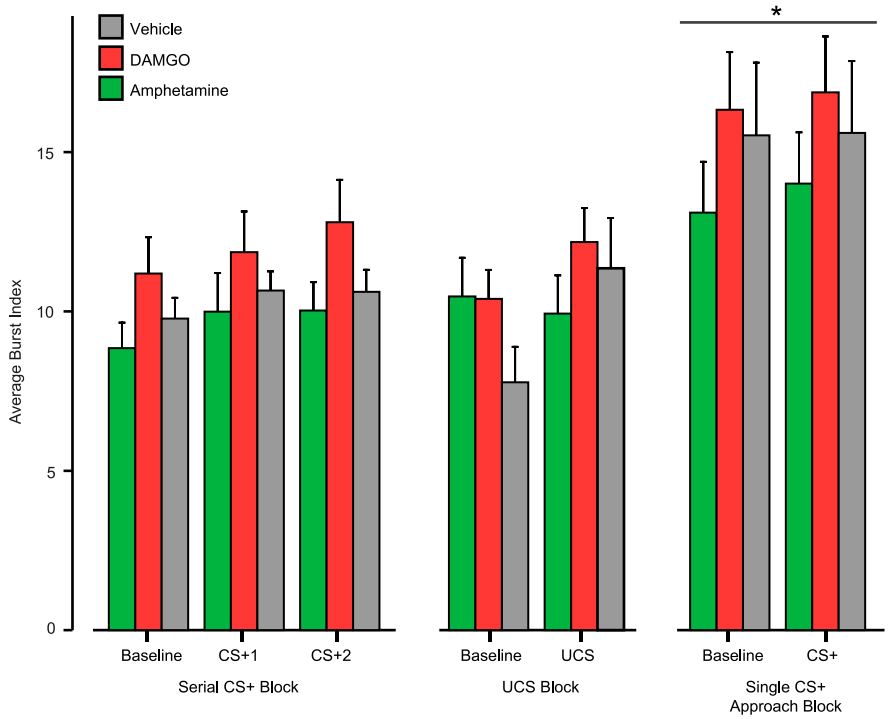

Fig. S7. Bursting properties of VP firing activity across task epochs, stimuli, and NAc microinjection conditions. Bursting rates (*SI Materials and Methods* and *SI Results*) were generally stable across the experiments, with the exception that bursting increased during the single CS+ approach block of trials compared with earlier task epochs, independently of NAc microinjection.